INTERNATIONAL JOURNAL FOR NUMERICAL METHODS IN FLUIDS, VOL. 16, 759–775 (1993)

ON THE ACCURACY AND EFFICIENCY OF CFD METHODS IN REAL GAS HYPERSONICS

D. DRIKAKIS

Lehrstuhl für Strömungsmechanik, Universität Erlangen-Nürnberg, Cauerstrasse 4, D-8520, Erlangen, Germany

AND

S. TSANGARIS

National Technical University of Athens, PO Box 640 70, 157 10 Zografou, Athens, Greece

SUMMARY

A study of viscous and inviscid hypersonic flows using generalized upwind methods is presented. A new family of hybrid flux-splitting methods is examined for hypersonic flows. The hybrid method is constructed by the superposition of the flux-vector-splitting (FVS) method and second-order artificial dissipation in the regions of strong shock waves. The conservative variables on the cell faces are calculated by an upwind extrapolation scheme to third-order accuracy. A second-order-accurate scheme is used for the discretization of the viscous terms. The solution of the system of equations is achieved by an implicit unfactored method. In order to reduce the computational time, a local adaptive mesh solution (LAMS) method is proposed. The LAMS method combines the mesh-sequencing technique and local solution of the equations. The local solution of either the Euler or the Navier–Stokes equations is applied for the region of the flow field where numerical disturbances die out slowly. Validation of the Euler and Navier–Stokes codes is obtained for hypersonic flows around blunt bodies. Real gas effects are introduced via a generalized equation of state.

KEY WORDS Euler/Navier–Stokes equations Hypersonic flows Real gas Upwind scheme

1. INTRODUCTION

The development of computational methods for hypersonic flows has attracted increasing interest in recent last years. CFD is expected to play an important role in hypersonic vehicle design because of the difficulties in producing data from experimental facilities. The focus of CFD methods is on the accurate simulation of flows with strong shock waves, capturing complex flow phenomena and variations in the variables for hypersonic flows.

The study of hypersonic shock waves around a blunt body constitutes one of the major problems in hypersonic aerodynamics, because the blunt shape is used to reduce heat transfer, especially in the nose of the body. The shock wave is stronger in front of the body, while large variations in the flow variables occur across it.

Numerical methods must capture these variations in the thin shock and entropy layer and in the thick boundary layers, as well as the viscous interaction.[1,2] During the last 15 years many upwind methods have been developed for transonic and supersonic flows. These methods have improved the accuracy of the numerical solution for both inviscid and viscous flows.[3–8] Despite

0271–2091/93/090759–17$13.50

Received June 1992
Revised October 1992

the reliability of these methods, problems have arisen in their application to flows with strong shock waves, such as blunt body hypersonic flows.

Because of the high speed in hypersonic computations, numerical errors lead to negative values of the flow variables, such as negative pressures or spurious oscillations if the mesh lines are not aligned with the shock wave.[9] Many researchers have presented recent modifications of previous numerical methods for applications in hypersonic flows.[6,8,10,11]

Despite the above modifications, certain numerical problems still arise in hypersonic flow simulation.[9] Such problems are the spurious non-physical oscillation of the numerical solution in the region of strong shocks, errors in the conservation of the total temperature as well as the development of accurate thermodynamic models in order to include real gas effects in the numerical simulation. In the present work a new family of hybrid flux-splitting methods is examined for viscous and inviscid hypersonic flows. The hybrid method constructs the fluxes as a superposition of the splitting scheme and a second-order artificial dissipation model. The conservative variables on the cell faces can be calculated either by a five-point upwind scheme[12] or by the well-known MUSCL scheme.[13] Thus hybrid FVS methods are created up to fourth-order accuracy for the inviscid flux discretization. A second-order-accurate model is used for the discretization of the viscous fluxes.[14]

One of the major problems during the numerical solution of hypersonic flows is the slow rates of convergence of the numerical algorithms. In hypersonic flows small CFL numbers are required to capture slowly moving shock waves. It is known from experience in transonic and supersonic flows that unfactored solution methods including Gauss–Seidel relaxation allow the use of high CFL numbers. Numerical experiments have shown that high CFL numbers cannot be used in hypersonic flows even in the case where unfactored Newton-type methods[15,16] are used for the inversion of the system of equations. In order to reduce the computational time, a local solution method (LSM) is presented. This method was developed in the past to accelerate the convergence of the Euler and Navier–Stokes codes in transonic and supersonic flows, leading to a significant reduction in the computational time.[17] Extension of the LSM to hypersonic flows is presented.

Validation of the methods is obtained for hypersonic flows around blunt bodies for perfect and real gas equilibrium air.

2. GOVERNING EQUATIONS

The governing equations are the time-dependent Navier–Stokes equations for a compressible fluid. The equations can be written in conservation dimensionless form and for a generalized co-ordinate system as

$$JU_t+(E_{\text{inv}})_\xi+(G_{\text{inv}})_\zeta=\frac{1}{Re}[(E_{\text{vis}})_\xi+(G_{\text{vis}})_\zeta], \tag{1}$$

where Re is the Reynolds number, $U=(\rho, \rho u, \rho w, e)^{\mathrm{T}}$ is the conservative solution unknown vector and ρ, u, w and e are the density, velocity in the x-direction, velocity in the z-direction and total energy per unit volume respectively. E_{inv} and G_{inv} are the inviscid flux vectors and E_{vis} and G_{vis} are the viscous flux vectors. $J=x_\xi z_\zeta-z_\xi x_\zeta$ is the Jacobian of the transformation from Cartesian co-ordinates (x, z) to generalized co-ordinates (ξ, ζ).

The dimensionless viscosity μ can be defined for a real gas as a function of the density ρ and the specific internal energy i, i.e.

$$\mu=\mu(\rho, i), \tag{2}$$

while the Prandtl number Pr can be defined as a function of the temperature and the density, i.e.

$$Pr = Pr(T, \rho). \tag{3}$$

The formulation of the governing equations is completed by an equation of state:

$$p = p(\rho, i). \tag{4}$$

The implementation of the real gas properties into the numerical algorithm will be presented in a later section of the paper.

3. GENERALIZED FVS METHOD FOR HYPERSONIC FLOWS

Almost all upwind methods make use of operator splitting for the discretization of the inviscid fluxes. The use of highly accurate multidimensional upwind methods[18] is difficult for code development as well as very expensive in computational time. Because of the use of operator splitting, the solvers find it difficult to recognize strong variations which are not aligned with the mesh lines. This problem has also been observed by other authors[9,11] in flows with strong shock waves. In such flows many of the parameters take very small values, and if the solution is not accurate, negative square root arguments will blow up the solution. This latter effect is much stronger in the transient phase when the shock wave is moved.

This problem can be ovecome by increasing the artificial dissipation of the algorithm. In the present study the discretization of the inviscid fluxes is carried out by a modified Steger–Warming FVS method.[19] The FVS method decomposes the inviscid flux into two parts, positive and negative, in accordance with the signs of the eigenvalues:

$$(E_{\text{inv}})_{i+1/2} = (T\Lambda^+ T^{-1})_{i+1/2} U^-_{i+1/2} + (T\Lambda^- T^{-1})_{i+1/2} U^+_{i+1/2}, \tag{5}$$

where T and T^{-1} are the left and right eigenvector matrices respectively and Λ^+ and Λ^- are the positive and negative eigenvaliue matrices respectively. The split fluxes are defined on the cell faces of the computational volume instead of at the centre of the volume, because the first formulation improves the results in the boundary layer.[8,20]

The eigenvalues of the positive and negative eigenvalue matrices are split in accordance with Eberle *et al.*:[10]

$$\lambda_0^{\pm} = \frac{\lambda_1^{\pm} + \lambda_2^{\pm}}{2}, \tag{6a}$$

$$\lambda_j^{\pm} = \frac{\lambda_j + |\lambda_j|}{2}, \quad j = 1, 2, \tag{6b}$$

where

$$\lambda_0 = u\tilde{\xi}_x + w\tilde{\xi}_z, \qquad \lambda_1 = \lambda_0 + S, \qquad \lambda_2 = \lambda_0 - S,$$

with S representing the speed of sound. Splitting of the zeroth eigenvalue in accordance with equation (6a) reduces the errors related to the conservation of the total temperature. The split convective fluxes can be defined as

$$(E^{\text{FVS}}_{\text{inv}})^{\pm}_{i+1/2} = \rho |\nabla \xi| \begin{vmatrix} \frac{1}{2}(\lambda_1^{\pm} + \lambda_2^{\pm}) \\ (u + S\tilde{\xi}_x/\gamma)\,\lambda_1^{\pm}/2 + (u - S\tilde{\xi}_x/\gamma)\,\lambda_2^{\pm}/2 \\ (w + S\tilde{\xi}_z/\gamma)\,\lambda_1^{\pm}/2 + (w - S\tilde{\xi}_z/\gamma)\,\lambda_2^{\pm}/2 \\ \frac{1}{2} H^{\pm}(\lambda_1^{\pm} + \lambda_2^{\pm}) \end{vmatrix} J, \tag{7}$$

with

$$\tilde{\xi}_x=\frac{\xi_x}{\sqrt{(\xi_x^2+\xi_z^2)}}, \qquad \tilde{\xi}_z=\frac{\xi_z}{\sqrt{(\xi_x^2+\xi_z^2)}}.$$

As mentioned above, in order to overcome the numerical problems in hypersonic flow computations, artificial dissipation is added in the FVS method.

Because the zeroth eigenvalue is close to zero and the first and second eigenvalues do not have large variations in the stagnation regions, they are good indicators for the second-order damping terms. Thus the following model is constructed:

$$(D_\xi^2 U)_{i+1/2}=(cr_{i+1/2})\Delta_\xi U_{i,j}, \tag{8a}$$

$$r_{i+1/2}=\max(\Delta_\xi L_0, \Delta_\xi L_1, \Delta_\xi L_2, \varepsilon). \tag{8b}$$

The terms L_0, L_1, and L_2 are defined as

$$L_j=\frac{\lambda_j}{\sum_j |\lambda_j|}, \qquad j=0, 1, 2. \tag{9}$$

The parameter c is a constant with typical values between 0·05 and 0·18, while ε is a very small, positive constant number ($\varepsilon=10^{-5}$). The above model adds only a very small amount of second-order artificial dissipation in the shock region.

The generalized flux for hypersonic flows can be defined as

$$(E_{\text{inv}})_{i+1/2}=(E_{\text{inv}}^{\text{FVS}})_{i+1/2}+(D_\xi^2 U)_{i+1/2}. \tag{10}$$

The above flux can also be used in transonic and supersonic flows by setting the constant c in expression (8a) equal to zero.

4. HIGH-ORDER EXTRAPOLATION SCHEMES

The conservative variables on the cell faces can be calculated either by a hybrid five-point upwind extrapolation scheme[12] or by the well-known MUSCL scheme.[13] The hybrid five-point upwind scheme is constructed by superposition of the first-, second-, third- and fourth-order extrapolation schemes:

$$U_{i+1/2}^{\pm}=AU^{1,\pm}+(1-A)\{BU^{2,\pm}+(1-B)[CU^{3,\pm}+(1-C)]U^{4,\pm}\}. \tag{11}$$

The superscripts 1, 2, 3 and 4 denote the various orders of extrapolation. For instance, the third- and fourth-order extrapolations are defined as

$$(U_{i+1/2}^3)^-=\tfrac{1}{6}(5U_i-U_{i-1}+2U_{i+1}), \qquad (U_{i+1/2}^3)^+=\tfrac{1}{6}(5U_{i+1}-U_{i+2}+2U_i),$$

and

$$(U_{i+1/2}^4)^-=(U_{i+1/2}^4)^+=\tfrac{1}{2}(7U_i+7U_{i+1}-U_{i-1}-U_{i+2})$$

respectively.

The terms A and B are limiter functions and are defined by the second-order derivatives of the pressure:[12]

$$A=\min(1, d|P_{\xi\xi,i+1}^2-P_{\xi\xi,i}^2|), \tag{12a}$$

$$B=\min(1, b|P_{\xi\xi,i+1}^2-P_{\xi\xi,i}^2|). \tag{12b}$$

The values of the constants are $d=4·5$, $b=2·5$ and $C=2·25$.

The second approach to the calculation of the conservative variables on the cell faces is the MUSCL scheme.[13]

Numerical experiments[20] have shown that the hybrid upwind and MUSCL schemes present similar behaviour for inviscid flows. For viscous flows the MUSCL scheme in combination with the FVS method leads to inaccuracies in the boundary layers,[21,22] while the third-order hybrid scheme captures the skin friction and velocity distribution in the boundary layers with satisfactory accuracy. In accordance with the above, the hybrid upwind scheme is used for viscous flows.

5. UNFACTORED IMPLICIT RELAXATION SOLUTION

An unfactored implicit method is used in combination with the generalized FVS method for the solution of the system of equations. The implicit method is first-order-accurate in time. The unfactored equations are solved via a Newton-type method by constructing a sequence of approximations q^ν such that

$$\lim_{\nu>1} q^\nu \to U^{n+1},$$

where ν is the subiteration state. A Newton form is obtained by linearization of equation (1) around the known subiteration state ν as follows:

$$J\frac{\Delta q^{\nu+1}}{\Delta t}+(A^\nu_{\text{inv}}\,\Delta q^{\nu+1})_\xi+(C^\nu_{\text{inv}}\,\Delta q^{\nu+1})_\zeta+(C^\nu_{\text{vis, th}}\,\Delta q^{\nu+1})_\zeta=J\frac{U^n-q^\nu}{\Delta t}-\text{RHS}, \tag{13a}$$

where

$$\text{RHS}=(E^\nu_{\text{inv}})_\xi+(G^\nu_{\text{inv}})_\zeta-\frac{1}{Re}(E^\nu_{\text{vis}})_\xi-\frac{1}{Re}(G^\nu_{\text{vis}})_\zeta \tag{13b}$$

and q^ν and $q^{\nu+1}$ are the solution vectors at the subiteration states ν and $\nu+1$ respectively. Gauss–Seidel relaxation using four subiteration states is applied on the LHS of equation (13a) while the RHS is held constant.[16] On the LHS the thin layer viscous Jacobian $C_{\text{vis, th}}$ is used for steady state calculations, saving computational time. The inviscid fluxes on the LHS of equation (13a) are split as follows:

$$(A^\nu_{\text{inv}}\,\Delta q^{\nu+1})_\xi=(A^\nu_{\text{inv}}\,\Delta q^{\nu+1})_{i+1/2}-(A^\nu_{\text{inv}}\,\Delta q^{\nu+1})_{i-1/2},$$

$$(A^\nu_{\text{inv}}\,\Delta q^{\nu+1})_{i+1/2}=(T\Lambda^+T^{-1})^\nu_{i+1/2}\,(\Delta q^{\nu+1})^+_{i+1/2}+(T\Lambda^-T^{-1})^\nu_{i+1/2}\,(\Delta q^{\nu+1})^-_{i+1/2},$$

with

$$(\Delta q^{\nu+1})^+_{i+1/2}=b\Delta q^{\nu+1}_i+\tfrac{1}{2}(1-b)(3\Delta q^{\nu+1}_i-\Delta q^{\nu+1}_{i-1}),$$

$$(\Delta q^{\nu+1})^+_{i+1/2}=(\Delta q^{\nu+1})_{i+1}.$$

The parameter b is a function defined from the values of the RHS in order to decrease the accuracy of the extrapolation in the regions of discontinuities. In order to retain the stability of the implicit solution, the split eigenvalue matrices are defined as

$$\Lambda^+=\max(F,\Lambda), \qquad \Lambda^-=\min(-F,\Lambda),$$

where

$$F=Bh\max[|\lambda_1|,|\lambda_2|].$$

The sensor B is defined by equation (12b) if the hybrid upwind scheme is used for the discretization of the inviscid fluxes. If the FVS method is used with the MUSCL upwind scheme, the sensor B is better defined by the squares of the Mach number on the left and right states of the cell face. The constant h is 0·5.

6. LOCAL SOLUTION METHOD

As mentioned in Section 1, slow rates of convergence have been observed in numerical simulations of hypersonic flow fields. In order to reduce the computational time, a combination of the mesh-sequencing technique with a local solution method is applied. In the mesh-sequencing technique[17,23] an initial guess on the fine mesh is obtained by first iterating the solution of the equations on a sequence of coarser grids and then interpolating the solution to the next finer grid. In the present calculations two levels (coarse and fine meshes) have been used. The coarse mesh is constructed by eliminating every second line of the fine mesh in each direction. Because in the mesh-sequencing procedure the centres of the volumes of the fine mesh are not a subset of the volumes of the coarse mesh, bilinear interpolation is used for the calculation of the conservative variables from the corresponding variables of the coarse mesh.

In accordance with the non-uniform propagation of the numerical disturbances,[24] the solution of the equations can be obtained only in the region of the flow field where the disturbances are large (exceed a prescribed value), while the rest of the flow field is considered to be converged. Drikakis and Tsangaris[17] have observed that the numerical disturbances decrease rapidly away from the solid boundary and the shock wave regions in transonic and supersonic flows.

In the case of hypersonic flow around a blunt body the shock wave is formed near the solid boundary and thus interaction between the solid boundary and the shock wave in inviscid flows as well as between the shock wave and the thick boundary layer in viscous flows occurs. The behaviour of the numerical disturbances has been studied separately for the inviscid and viscous flow cases. The basic conclusions from this study are as follows. In inviscid hypersonic flows the numerical disturbances are diminished faster from the solid boundary region (except for the stagnation region) than from the region of the slowly moving shock wave. During the numerical solution the shock wave is moved until its final steady state position is achieved. After the steady state position of the shock, numerical disturbances continue to exist in the region of large variations until the achievement of the final steady state values of the variables across the shock wave. In accordance with the above, local solutions can be achieved in the region around the shock wave and in front of the body nose, during the numerical iterations.

In viscous hypersonic flows large values of the numerical disturbances are present (after a number of iterations) in the boundary layer and around the shock wave. Thus two local solution zones are constructed. The first overlaps the bow shock wave while the second overlaps a part of the boundary layer around the body. The region between the two zones is frozen until the steady state solution is achieved in the whole flow field. The local solution regions are generated by an adaptation procedure.[17]

7. INCORPORATION OF REAL GAS EFFECTS

Extensions of FVS methods to deal with real gas effects have been presented by several authors.[25,28] It is known that if we consider the pressure as a function of the density and the specific internal energy, the Steger–Warming FVS method does not satisfy the homogeneous property of the Euler equations. Thus the incorporation of the real gas model is achieved by a parametrization, introducing an equivalent ratio of specific heats, $\tilde{\gamma}$, defined as

$$\tilde{\gamma}(\rho, i) = 1 + \frac{p(\rho, i)}{\rho i}.$$

The generalized equation of state and the equations for the transport properties (viscosity, thermal conductivity, Prandtl number) have been developed by Srinivasan and co-workers.[29,30]

The true speed of sound can be expressed via the introduction of pressure derivatives as

$$S^2 = p_\rho + p\frac{p_i}{\rho^2}, \tag{14}$$

where p_ρ and p_i are the pressure derivatives with respect to the density and the specific internal energy respectively. Instead of using the latter equation, the speed of sound can be expressed in terms of the equivalent ratio $\tilde{\gamma}$ as

$$S^2 = \tilde{\gamma}(\rho, i)\frac{p}{\rho}$$

Using the above equation, computational time is saved in comparison with the use of equation (14), where the pressure derivatives must be calculated approximately.[27,28]

In order to save computational time, the ratio $\tilde{\gamma}$ and the transport properties of the air are updated every fifth iteration. This process does not affect the stability of the numerical solution.

Although the split fluxes on the RHS require no significant modifications for the real gas model, a different approach on the LHS of equation (13a) can be used by the derivation of the Jacobian matrices and eigenvectors for a general equation of state.[28] This approach makes the Jacobians and eigenvectors as functions of the pressure derivatives. Numerical experiments for the present hypersonic flows showed that the above procedure increases the CPU time but does not have any influence on the numerical results. Thus the equivalent ratio $\tilde{\gamma}$ is also used in the implicit part of the method (equation (13a)).

8. RESULTS

Validation of the Euler and Navier–Stokes codes is obtained for hypersonic flows around blunt bodies, because these geometries are particularly important shapes in hypersonic aerodynamics.

Initially, the efficiency of the local solution method (LSM) has been tested for a hypersonic inviscid flow with $M = 6{\cdot}3$ around a cylinder. A physical picture of the flow field is shown in Figure 1(a). The mesh sequencing, the LSM and the influence of the relaxation factor (in the Gauss–Seidel relaxation sweeps) in the convergence have been studied. In transonic and supersonic flows ($M_\infty \leqslant 2$) the relaxation factor (RL) has the value 0·2. For the present flow the mesh-sequencing procedure has been tested using $RL = 0{\cdot}2$ and 0·6. From Figure 1(b) it is obvious that the value $RL = 0{\cdot}6$ improves the convergence. In the same figure it is also shown that the mesh-sequencing procedure reduces the computational work in comparison with the fine mesh. The mesh-sequencing method has also been used in combination with the LSM. After convergence of the solution on the coarse mesh (residual $\approx 10^{-6}$), the iterations are continued on the fine mesh. The local solution is applied when the residual reaches a value of about 10^{-3}. The convergence of the equations on the partial meshes is faster than the convergence on the fine mesh (using mesh sequences). Thus after 450 iterations convergence has been achieved by the LSM, while using only the mesh-sequencing procedure 720 iterations are required. Hence a combination of the mesh-sequencing method and the LSM is used for the calculation of the present hypersonic flow fields.

An inviscid case is considered for validation of the perfect and real gas versions of the code, namely a hypersonic flow with a freestream Mach number of 15 over a blunt body. The above flow field was also calculated by Grossman and Walters[31] using Roe's flux-difference-splitting method. In Figure 2 the 81×41 computational mesh is shown. Reference conditions were chosen to correspond to atmospheric conditions at an altitude of 45 km: $p = 170\ \mathrm{N\,m^{-2}}$, $\rho = 0{\cdot}002\ \mathrm{kg\,m^{-3}}$, $T = 295$ K.

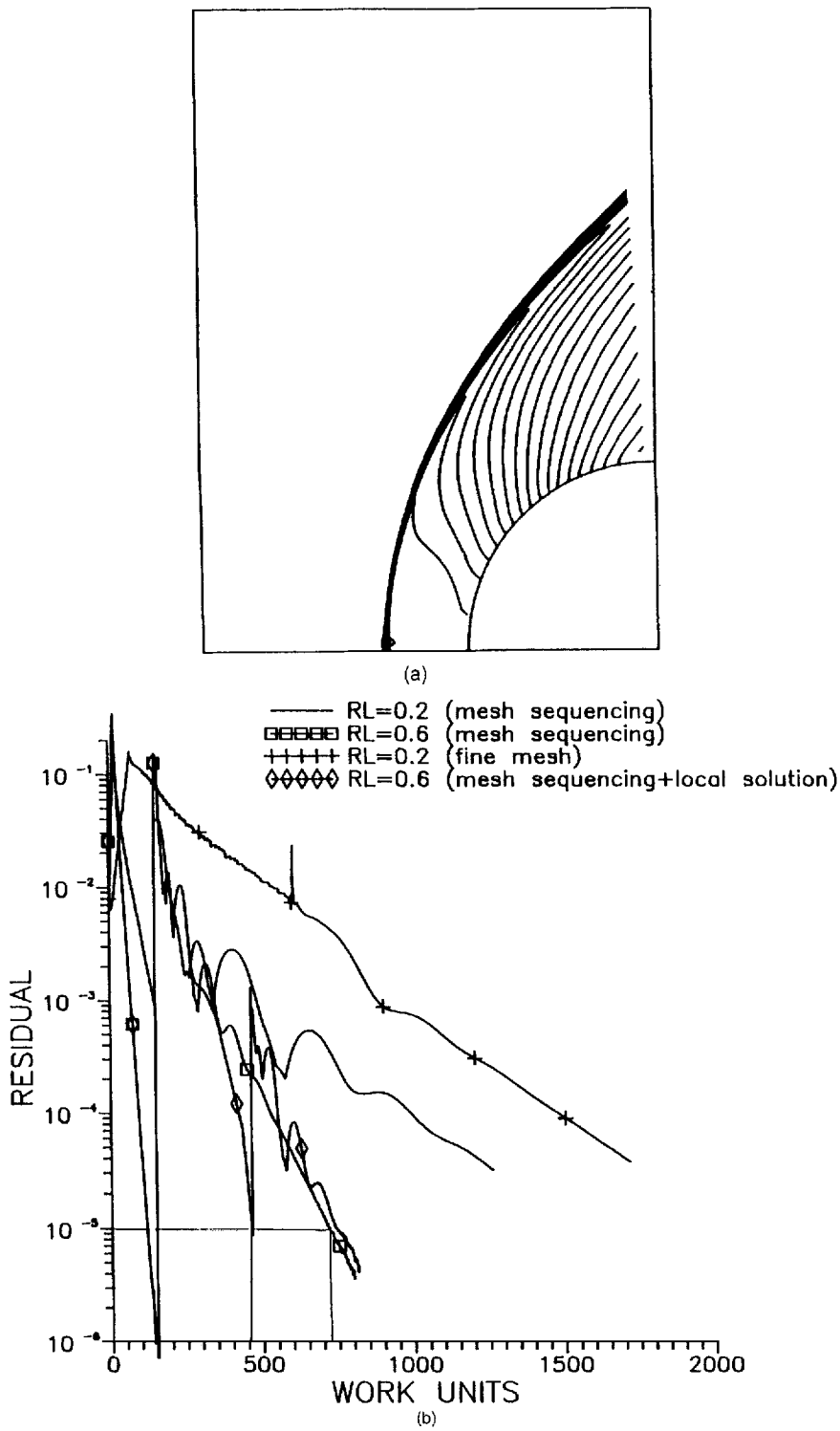

Figure 1. Hypersonic flow with $M = 6{\cdot}3$ around a cylinder: (a) isodensity lines, (b) convergence histories

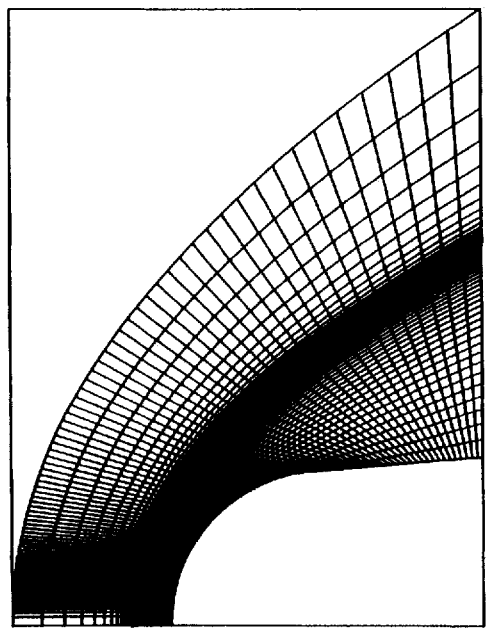

Figure 2. Computational mesh (81 × 41) for inviscid hypersonic flow with $M = 15$

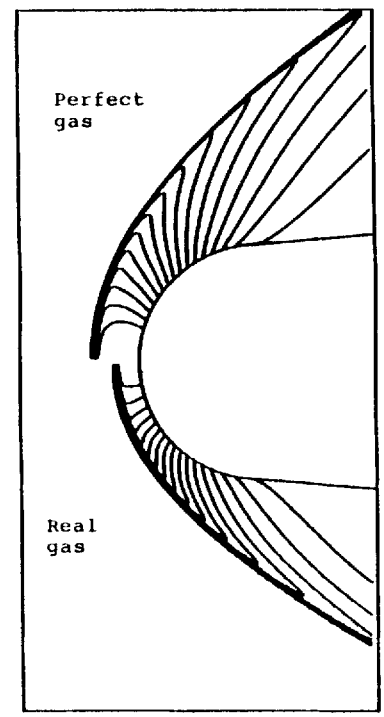

Figure 3. Isopressure lines for perfect and equilibrium air (inviscid hypersonic flow, $M = 15$)

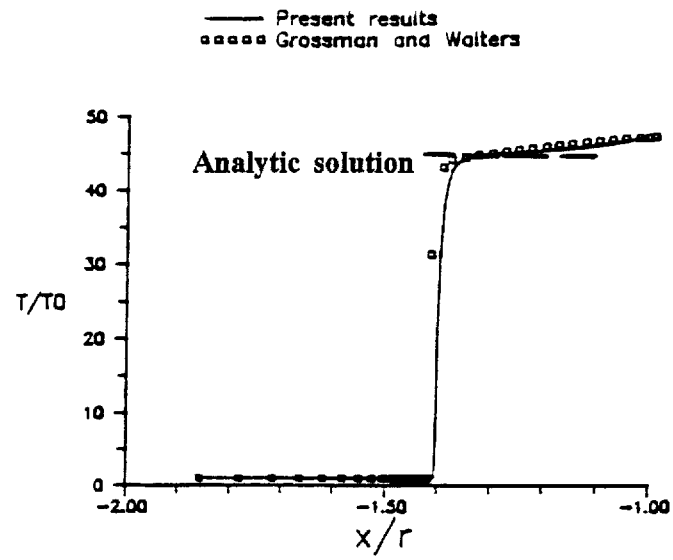

Figure 4. Temperature distribution along symmetry line (inviscid hypersonic flow, $M = 15$)

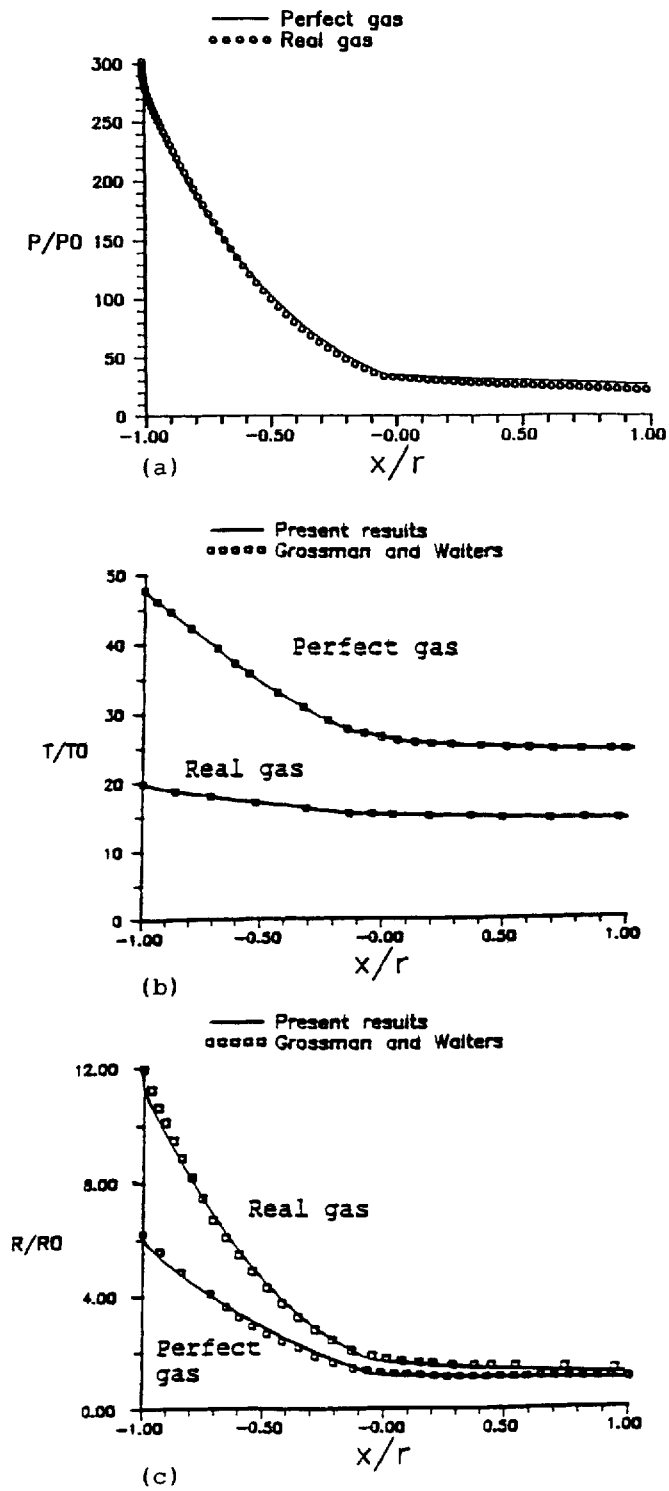

Figure 5. Distributions along body surface: (a) pressure, (b) temperature, (c) density (inviscid hypersonic flow, $M = 15$)

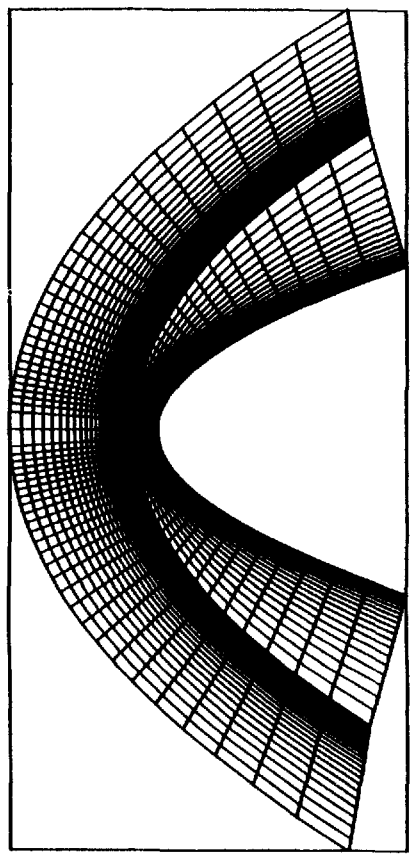

Figure 6. Computational mesh (60 × 60) for viscous hypersonic flow ($M=10$, $Re=1{\cdot}2\times10^4$) around a hyperbola

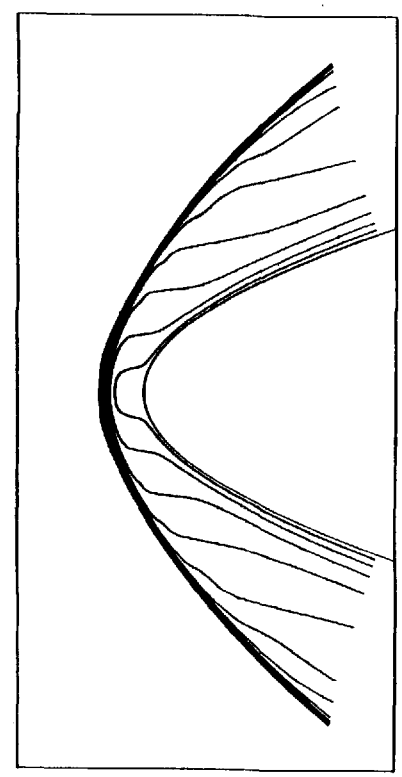

Figure 7. Iso-Mach lines around hyperbola ($M=10$, $Re=1{\cdot}2\times10^4$)

For the real gas calculations the thermodynamic subroutines of Srinivasan and coworkers[29,30] have been used. The isopressure lines for the perfect and real gas calculations are shown in Figure 3. The resolution of the shock waves is very good. The pressure contours show large differences in the stand-off distance between perfect and equilibrium air. In Figure 4 the temperature distribution along the symmetry line is plotted. The present results are compared with the corresponding results of Grossman and Walters.[31] The jump in the flow values across the shock wave is also compared with the analytic solution. The calculated stand-off distance $d=0{\cdot}401R$ is in good agreement with the corresponding experimental value $d=0{\cdot}3941R$ obtained by Billig.[32] In Figure 5 the pressure, temperature and density distributions along the body surface are shown. The influence of the real gas is significant in the temperature and density distributions. All the above results are in good agreement with the corresponding results from the literature.

Validation of the Navier–Stokes code for hypersonic flows has been obtained for a flow with a freestream Mach number $M=10$ and $Re=1{\cdot}2\times10^4$ around a hyperbola with the equation

$$\left(\frac{x}{500\text{ mm}}+1\right)^2-\left(\frac{y}{88\text{ mm}}\right)^2=1.$$

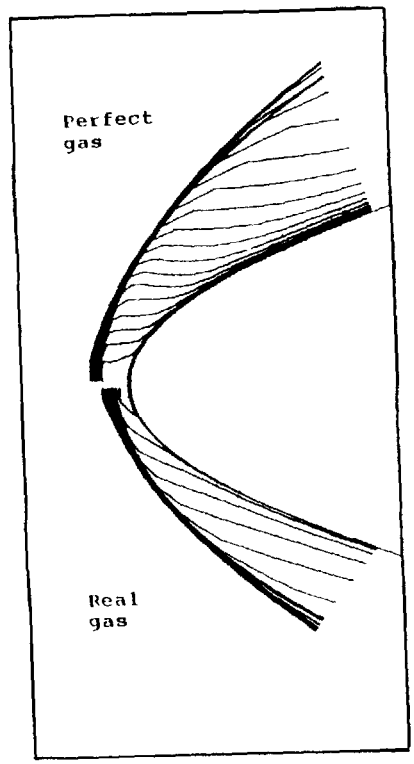

Figure 8. Isotemperature lines for perfect and equilibrium air ($M=10$, $Re=1{\cdot}2\times10^4$)

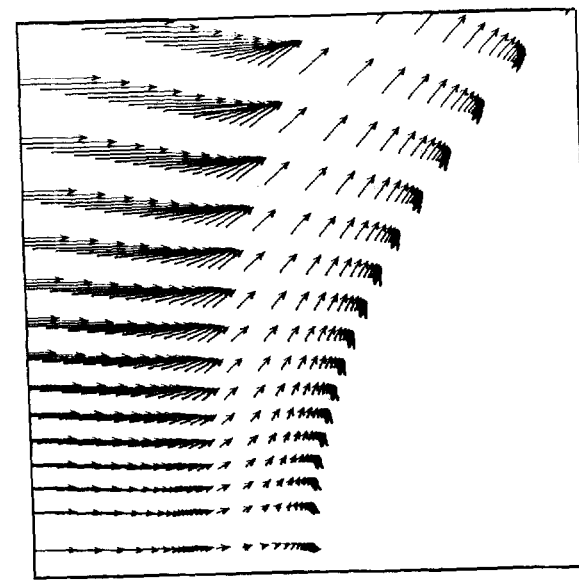

Figure 9. Velocity vectors in stagnation region of hyperbola for equilibrium air ($M=10$, $Re=1{\cdot}2\times10^4$)

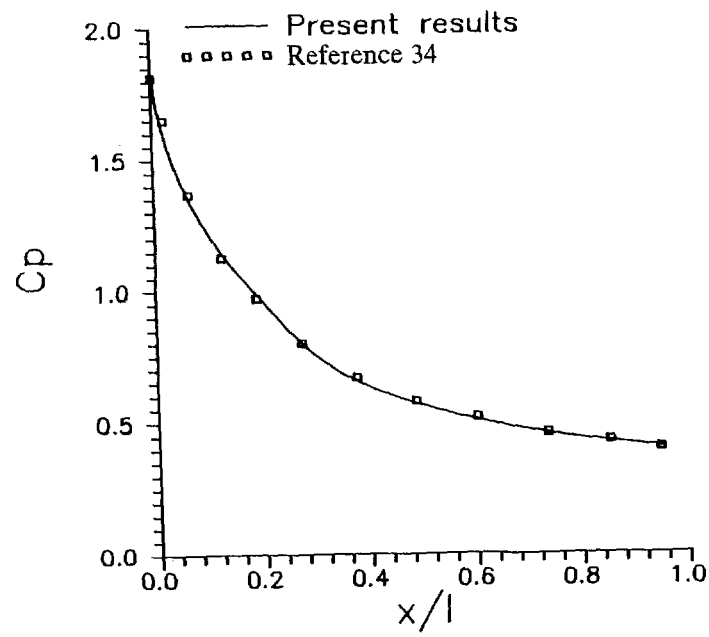

Figure 10. Pressure coefficient distribution (c_p) along hyperbola wall for perfect air ($M=10$, $Re=1{\cdot}2\times10^4$)

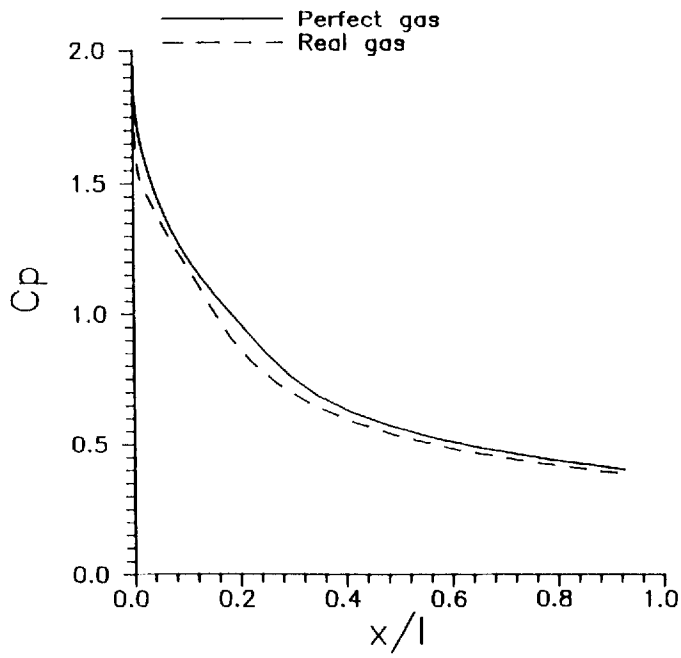

Figure 11. Comparison of c_p between perfect and equilibrium air ($M=10$, $Re=1{\cdot}2\times10^4$)

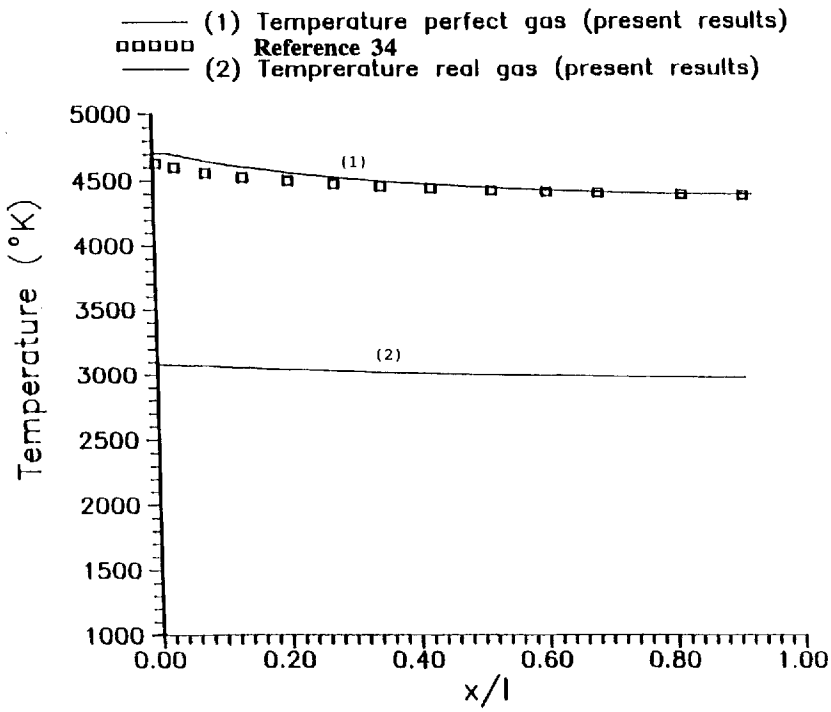

Figure 12. Temperature distributions along hyperbola wall ($M=10$, $Re=1{\cdot}2\times10^4$)

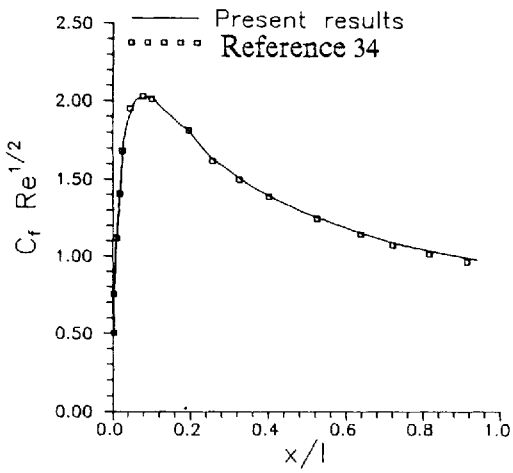

Figure 13. Skin friction distribution (c_f) along hyperbola wall for perfect air ($M=10$, $Re=1{\cdot}2\times10^4$)

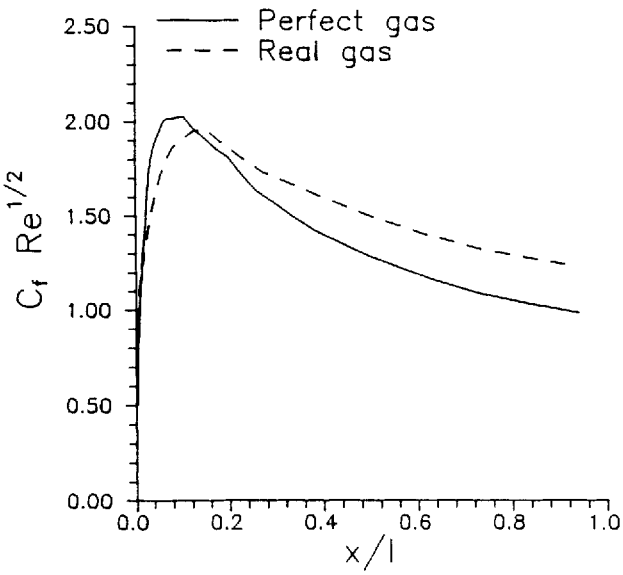

Figure 14. Comparison of c_f between perfect and equilibrium air

This hypersonic flow has also been studied by other authors.[33,34] Reference conditions were chosen to correspond to atmospheric conditions at an altitude of 52 km: $p=48{\cdot}67\ \mathrm{N\,m^{-2}}$, $\rho=7{\cdot}7\times10^{-4}\ \mathrm{kg\,m^{-3}}$, $T=225$ K. The wall of the hyperbola is considered adiabatic. The computational mesh is 60×60 (Figure 6). Iso-Mach lines are shown in Figure 7, while comparison of the flow field for perfect and equilibrium air is shown in Figure 8 as a plot of isotemperature lines. The resolution of the shocks is satisfactory. The code preserves the symmetry of the solution (Figure 7). It is noted that the calculations have been obtained in the whole flow field although the flow is symmetrical. The abrupt change in the flow direction in the region of strong variations is

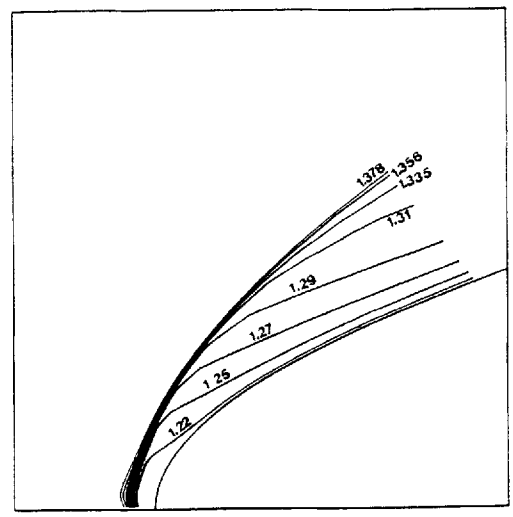

Figure 15. Variation in ratio $\tilde{\gamma}$ for viscous hypersonic flow

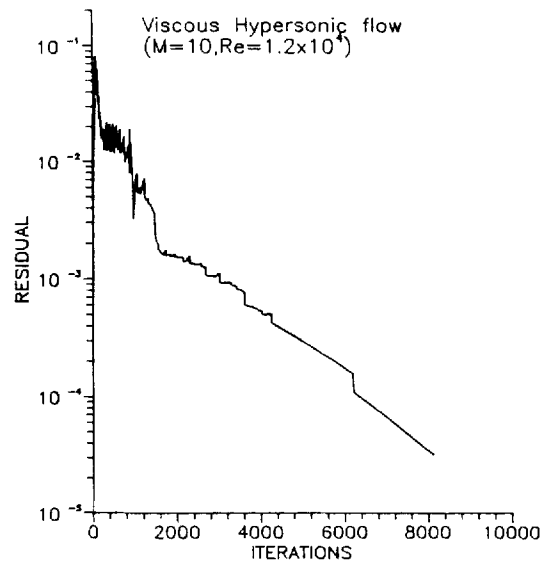

Figure 16. Convergence history for real gas viscous hypersonic flow ($M = 10$, $Re = 1{\cdot}2 \times 10^4$)

shown in Figure 9 for the real gas case. Comparisons between the present results and those of References 33 and 34 for the pressure coefficient, temperature and skin friction are shown in Figures 10–14.

The real gas effects are not significant in the pressure distribution (Figure 11) but are in the temperature field (Figure 12). The results for the pressure and skin friction distributions (Figures 10 and 13) are in good agreement with the corresponding results from the literature.[33,34] In Figure 15 the variation in the equivalent ratio $\tilde{\gamma}$ over the hyperbola is plotted. The convergence history (real gas calculation) is shown in Figure 16. The CPU time is 0·003 s per iteration per grid

point (on a SUN 1+). The number of iterations for the perfect and real gas calculations is the same, but the thermodynamic subroutines for equilibrium air increase the CPU time by about 20% for the real gas calculations.

9. CONCLUSIONS

The accuracy and efficiency of upwind hybrid FVS methods have been discussed and results for inviscid and viscous hypersonic flows have been presented. The conclusions are as follows.

1. The efficiency of the unfactored solution can be improved by using mesh sequencing and the local solution method.
2. The hybrid FVS method can capture strong shock waves with satisfactory accuracy.
3. The results with the Euler and Navier–Stokes codes are in satisfactory agreement with the corresponding results from the literature.

REFERENCES

1. W. D. Hayes and R. F. Probstein, *Hypersonic Flow Theory*, Academic, New York, 1959.
2. J. D. Anderson Jr. *Hypersonic and High Temperature Gas Dynamics*, McGraw-Hill, New York, 1982.
3. J. L. Steger and R. F. Warming, 'Flux vector splitting of the inviscid gas dynamic equations with applications to finite difference methods', *J. Comput. Phys.*, **40**, 263–293 (1981).
4. P. L. Roe, 'Approximate Riemann solvers, parameters vectors and difference schemes', *J. Comput. Phys.*, **43**, 357–372 (1981).
5. B. van Leer, 'Towards the ultimate conservative difference scheme. II. Monotonicity and conservation combined in a second order scheme', *J. Comput. Phys.*, **14**, 361–370 (1974).
6. H. C. Yee, 'Upwind and symmetric shock capturing schemes', *NASA-TM 89464*, 1987.
7. S. R. Chakravarthy, 'High resolution upwind formulations for the Navier–Stokes equations', *VKI Lecture Ser., Comput. Fluid Dyn., 1988-05*, 1988.
8. R. W. MacCormack and G. V. Candler, 'The solution of the Navier–Stokes equations using Gauss–Seidel relaxation', *Comput. Fluids*, **17**, 135–150 (1989).
9. W. Kordulla, 'Computational techniques for hypersonic flows', *AGARD 761*, 1988.
10. A. Eberle, M. A. Schmatz and N. C. Bissinger, 'Generalized flux vectors for hypersonic shock capturing', *AIAA Paper 90-0390, 28th Aerospace Sciences Meeting*, Reno, NV, 1990.
11. B. Müller, 'Simple improvements of an upwind scheme for hypersonic flows', *AIAA Paper 89-1977, 9th CFD Conf.*, Buffalo, NY, 1989.
12. A. Eberle, 'Characteristic flux averaging approach to the solution of the Euler's equations', *VKI Lecture Ser., Comput. Fluid Dyn., 1987-04*, 1987.
13. W. K. Anderson, J. L. Thomas and B. van Leer, 'Comparisons of finite volume flux vector splittings for the Euler equations', *AIAA J.*, **24**, 1453–1460 (1986).
14. S. R. Chakravarthy, K. Y. Szema, U. C. Goldberg and J. J. Gorski, 'Application of a new class of high accuracy TVD schemes to the Navier–Stokes equations', *AIAA Paper 85-0165*, 1985.
15. S. R. Chakravarthy, 'Relaxation methods for unfactored implicit upwind schemes', *AIAA Paper 84-0165, 22nd Aerospace Sciences Meeting*, Reno, NV, 1984.
16. M. A. Schmatz, A. Brenneis and A. Eberle, 'Verification of an implicit relaxation method for steady and unsteady viscous and inviscid flow problems', *AGARD CP-437*, 1988, pp. 15-1–15-33.
17. D. Drikakis and S. Tsangaris, 'Local solution acceleration method for the Euler and Navier–Stokes equations', *AIAA J.*, **30**, 340–348 (1992).
18. P. Colella, 'Multidimensional upwind methods for hyperbolic conservation laws', *J. Comput. Phys.*, **87**, 171–200 (1990).
19. D. Drikakis and S. Tsangaris, 'Laminar and turbulent viscous compressible flows using improved flux vector splittings', in J. B. Vos, A. Rizzi and I. L. Ryhming (eds), *Proc. 9th GAMM Conf. on Numerical Methods in Fluid Mechanics, Notes on Numerical Fluid Mechanics*, Vol. 35, Vieweg, Braunschweig, 1992, pp. 407–416.
20. D. Drikakis, 'Development of upwind numerical methods for high speed aerodynamics', *Ph.D. Dissertation*, National Technical University of Athens, 1991.
21. D. Hänel, R. Schwane and G. Seider, 'On the accuracy of upwind schemes for the solution of the Navier–Stokes Equations', *AIAA Paper 87-1105, 8th CFD Conf.*, Honolulu, HW, 1987.
22. B. van Leer, J. L. Thomas, P. L. Roe and R. W. Newsome, 'A comparison of numerical flux formulas for the Euler and Navier–Stokes equations', *AIAA Paper 87-1104, 8th CFD Conf.*, Honolulu, HW, 1987.
23. T. H. Pulliam, 'Efficient solution methods for the Navier–Stokes equations', *VKI Lecture Ser.*, 1986.

24. A. G. Panaras, 'The spatially non-uniform convergence of the numerical solution of flows', *J. Comput. Phys.*, **82,** 429–453 (1989).
25. B. Grossman and R. N. Walters, 'Flux-split algorithms for the multi-dimensional Euler equations with real gases', *Comput. Fluids*, **17,** 99–112 (1989).'
26. M. S. Liou, B. van Leer and J. S. Shuen, 'Splitting of inviscid fluxes for real gases', *J. Comput. Phys.*, **87,** 1–24 (1990).
27. P. Glaister, 'An approximate linearised Riemann solver for the three dimensional Euler equations', *J. Comput. Phys.*, **77,** 361–383 (1988).
28. D. Drikakis and S. Tsangaris, 'An implicit characteristic flux-averaging method for the Euler equations for real gases', *Int. j. numer. methods fluids*, **12,** 711–726 (1991).
29. S. Srinivasan and J. C. Tannehill, 'Simplified curve fits for the transport properties of equilibrium air', *NASA CR-178411*, 1987.
30. S. Srinivasan, J. C. Tannehill and K. J. Weilmuenster, 'Simplified curve fits for the thermodynamic properties of the equilibrium air', *NASA RP-1181*, 1987.
31. B. Grossman and R. N. Walters, 'Analysis of flux-split algorithms for the Euler's equations with real gases', *AIAA J.*, **27,** 524–532 (1989).
32. F. S. Billig, 'Shock-wave shapes around spherical and cylindrical nosed bodies', *J. Spacecr. Rockets*, **4,** 822–823 (1967).
33. M. A. Schmatz, 'Hypersonic three-dimensional Navier–Stokes calculations for equilibrium gas', *AIAA Paper 89-2183, 7th Applied Aerodynamics Conf.*, Seattle, WA, 1989.
34. C. H. Mundt, M. Pfintzer and M. A. Schmatz, 'Calculation of viscous hypersonic flows using a coupled Euler/2nd order boundary layer method', *MBB-FE122-S-PUB-387*, 1989.